SOFT ROBOTICS
Volume 00, Number 00, 2022

DOI: 10.1089/soro.2022.0013

SoRo
Soft Robotics

Open camera or QR reader and scan code to access this article and other resources online.

Electrostatic Adhesion Clutch with Superhigh Force Density Achieved by MXene-Poly(Vinylidene Fluoride–Trifluoroethylene–Chlorotrifluoroethylene) Composites

Daiyue Wei,[1,2,*] Quan Xiong,[1,2,*] Jiufeng Dong,[3,4] Huacen Wang,[1,2] Xuanquan Liang,[1,2] Shiyu Tang,[1,2] Xinwei Xu,[3] Hongqiang Wang,[1,2,5] and Hong Wang[3]

Abstract

Electrostatic adhesion (EA) clutches are widely applied in robots, wearable devices, and virtual reality, due to their compliance, lightweight, ultrathin profile, and low power consumption. Higher force density has been constantly perpetuated in the past decades since EA was initially proposed. In this study, by composing terpolymer poly(vinylidene fluoride–trifluoroethylene–chlorotrifluoroethylene) [P(VDF-TrFE-CTFE)] and two-dimensional $Ti_3C_2T_x$ nanosheets (MXene), nanocomposite films with high dielectric constant ($\varepsilon_r' > 2300$) and low loss tangent are achieved. The force representative index $\varepsilon_r' E_{bd}^2$ (the relative dielectric constant times the square of breakdown electric field) is enhanced by 5.91 times due to the charge accumulation at matrix–filler interfaces. Superhigh shear stress (85.61 N cm^{-2}) is generated, 408% higher than the previous maximum value. One of the EA clutches fabricated in this study is only 160 μm thin and 0.4 g heavy. Owing to the low current (<1 μA), the power consumption is <60 mW/cm^2. It can hold a 2.5 kg weight by only 0.32 cm^2 area and support an adult (45 kg) (Clinical Trial Registration number: 20210090). With this technology, a dexterous robotic hand is displayed to grasp and release a ball, showing extensive applications of this technique.

Keywords: electrostatic adhesion, P(VDF-TrFE-CTFE), MXene, composites, high-force density

[1]Southern Marine Science and Engineering Guangdong Laboratory (Guangzhou), Guangzhou, China.
[2]Shenzhen Key Laboratory of Biomimetic Robotics and Intelligent Systems, Department of Mechanical and Energy Engineering, Southern University of Science and Technology, Shenzhen, China.
[3]Shenzhen Engineering Research Center for Novel Electronic Information Materials and Devices, Department of Materials Science and Engineering, Southern University of Science and Technology, Shenzhen, China.
[4]State Key Laboratory for Mechanical Behavior of Materials, School of Electronic and Information Engineering, Xi'an Jiaotong University, Xi'an, China.
[5]Guangdong Provincial Key Laboratory of Human-Augmentation and Rehabilitation Robotics in Universities, Southern University of Science and Technology, Shenzhen, China.
*The authors contributed equally to this study.

Introduction

Electrostatic adhesion (EA) was an emerging adhering technique based on the electrostatic field in recent decades.[1] The simplest EA device consists of two electrodes and a dielectric layer between them. When a voltage is applied, charges are induced on the electrodes, and electrostatic attraction is generated (Fig. 1a).

Owing to the advantages of the ultrathin profile, high adaptability, as well as low power consumption compared with other adhesion mechanisms such as magnetic adhesion and vacuum suction, this technology has been widely employed in various fields, including the end effectors,[2,3] crawling and climbing robots,[4,5] artificial muscle actuator,[6] and virtual reality devices.[7,8] In addition, EA technology has been applied in soft robotics and wearable applications since the electrodes, and the dielectric layer, can be manufactured by flexible and soft materials.[7–9]

The dielectric materials are the essential component of EA devices. Most previous studies employed polyimide (PI), biaxially oriented polypropylene (BOPP), parylene, and polyethylene terephthalate (PET) as the dielectric layer. Still, since the dielectric constant of these materials is comparably low (<4), high voltage (typically >1 kV) is required in the application to generate a strong enough force. To enhance the force density and reduce the magnitude of the voltage, dielectric materials with a higher dielectric constant have been introduced into EA recently. For example, Luxprint, composed of $BaTiO_3$ particles, with a dielectric constant of 35,[7] was applied as the dielectric material of EA clutch on exoskeleton and obtained 1.25 N/cm^2 EA shear stress at only 240 V.[10]

Nevertheless, with a higher dielectric constant, there is always a lower breakdown field (Fig. 1b), since the polar molecular bonds are weakened and tend to breakdown due to the high local electric field in high-dielectric constant materials.[11] For a wide range of metal oxide dielectric materials, the breakdown field is inversely proportional to the dielectric constant to the power of ~ 0.5 [$E_{bd} = a(\varepsilon_r')^b$ (MV/cm), in which a is about 20, b is about –0.5] based on previous literature.[11,12]

Similar relationship also exists in polymers. Most of the common polymers, such as BOPP, PI, PET, polypropylene (PP), polycarbonate (PC), polyetherimide (PEI), poly(vinylidene fluoride–cotetrafluoroethylene) [P(VDF-TFE)], polyvinylidene fluoride (PVDF), poly(vinylidene fluoride–cohexafluoropropylene) [P(VDF-HFP)], and poly (vinylidene fluoride–cochlorotrifluoroethylene) [P(VDF-CTFE)] have a rather low dielectric constant (2–11) and ultrahigh breakdown field (200–700 MV/cm).[13] According to this theory, the largest EA shear stress was generated (21 N/cm^2) based on terpolymer poly(vinylidene fluoride–trifluoroethylene–chlorotrifluoroethylene) [P(VDF-TrFE-CTFE)].[7] For more extensive applications, higher force density is still desired, and new materials must be developed.

In this study, we develop nanocomposite dielectric layers with superhigh EA shear stresses at relatively low voltage. By compositing two-dimensional (2D) $Ti_3C_2T_x$ nanosheets (MXene, with high conductivity and aspect ratio) and terpolymer (high dielectric constant), we achieve a nanocomposite with a large dielectric constant (>2300) at a very low $Ti_3C_2T_x$ loading (only 2 wt%). Operating at 500 V (alternating current [AC], 10 Hz) and 70°C, the nanocomposite (17 μm thickness) could maximize the EA shear stress to 85.61 N/cm^2, which is 408% higher than the previous maximum value (21 N/cm^2).[7]

With such a high force density, the EA clutch is capable of holding a barbell piece of 2.5 kg with an ultrasmall area (0.32 cm^2) as well as an adult of $\sim$45 kg. It has also been designed as a transmission mechanism to actuate a gripper. Moreover, an EA clutch pair (2×9 cm) is as thin as 160 μm, weighs only 0.4 g, and its maximum power consumption is only 59.97 mW/cm^2. Even if the power of heater per area (503.58 mW/cm^2) is added, the total power consumption is only 563.55 mW/cm^2.

Materials and Methods

Modeling and principle

Under the AC condition, the relative permittivity is given by

$$\varepsilon_r^* = \varepsilon_r' - i\varepsilon_r'', \tag{1}$$

where ε_r' is the real part and is also called dielectric constant, which reflects the dielectric property of the insulator, including dielectric relaxation and space charge polarization. ε_r'' is the imaginary part and represents the energy loss during the charge and discharge process of the capacitor, which is resulted from the movement of free electrons.[14] The loss tangent is a ratio between dispersed energy and the charge stored by the clutch, which is defined as:

$$\tan\delta = \frac{\varepsilon_r''}{\varepsilon_r'}. \tag{2}$$

In the electrostatic adhesive model (Fig. 1a), the force density perpendicular to the electrode plate is expressed by

$$f_\perp = \frac{1}{2}\varepsilon_0\varepsilon_r'\frac{V^2}{d^2} = \frac{1}{2}\varepsilon_0\varepsilon_r' E^2, \tag{3}$$

where ε_0 is the vacuum dielectric constant, V is the voltage applied on electrodes, d is the thickness of the dielectric layer, and E is the electrical field. The EA shear stress is the friction resulting from the electrostatic adhesive force

$$f_s = \mu f_\perp \le K\left(\varepsilon_r' E_{bd}^2\right), \tag{4}$$

where μ is the coefficient of friction, E_{bd} is the breakdown field or breakdown strength of the dielectric layer, and K is a constant ($K = \frac{1}{2}\mu\varepsilon_0$). Accordingly, the maximum EA shear stress is only determined by the two material properties, that is, the relative dielectric constant and the breakdown strength. Thus, we can improve the force density by trading off the two properties.

Material selection

Compared with ceramics, the polymer is our priority choice for the dielectric layer because it is soft, lightweight, and easy to be manufactured to film with variable thicknesses. Relaxor ferroelectric P(VDF-TrFE-CTFE) with a large dielectric constant ($\sim$40) is chosen.[7] This polymer has slim electric displacement–electric field (D-E) loops and small hysteresis due to the formation of nanodomains by incorporating large termonomers CTFE into P(VDF-TrFE) and is expected to have very high energy densities.[15] Two-

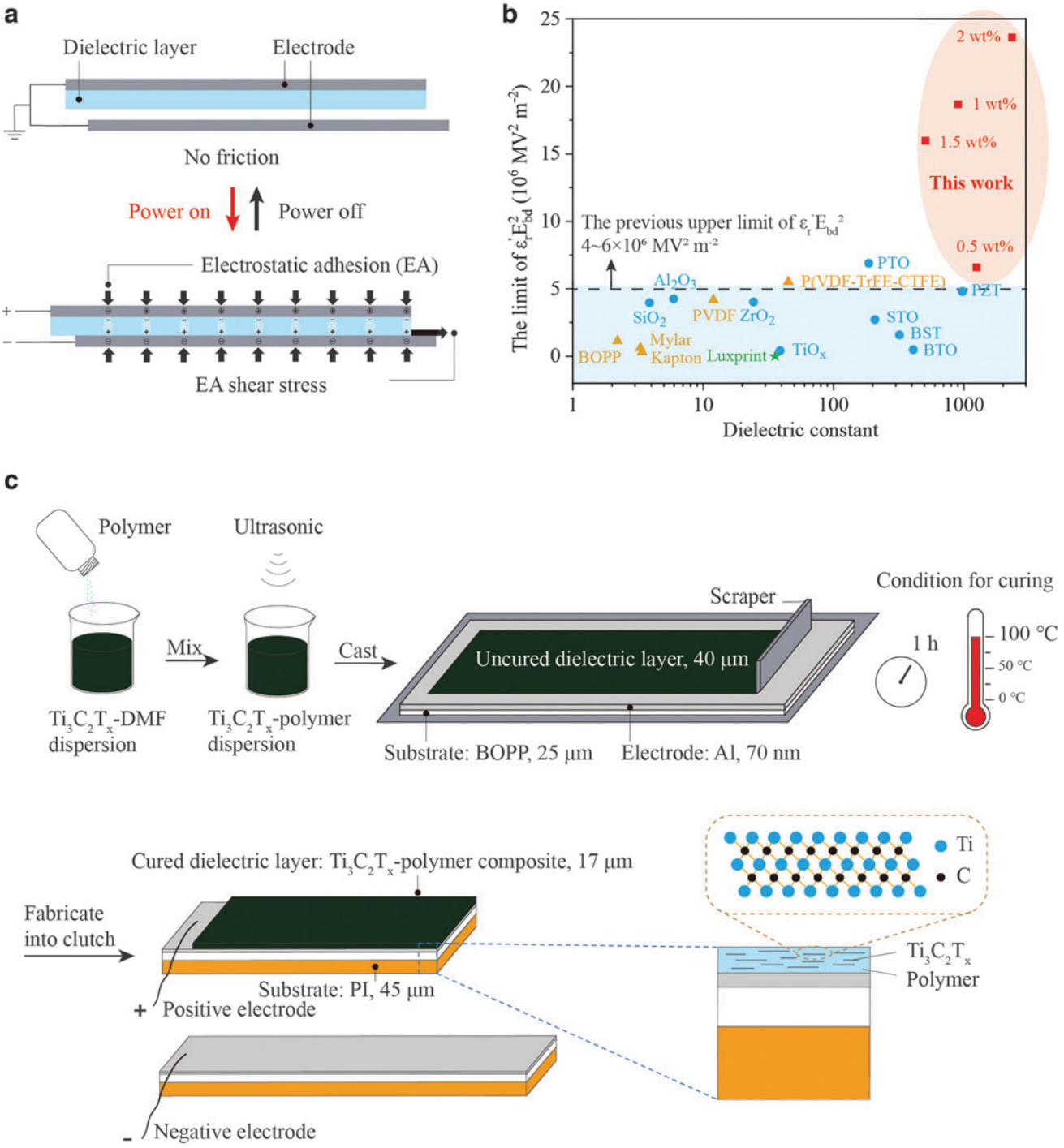

FIG. 1. The principle and fabrication of the EA clutch. **(a)** Sketch map of an EA clutch at two different states (power on and power off). **(b)** The upper limit of $\varepsilon_r' E_{bd}^2$ for different dielectric materials. This figure is revised from **G** in Ref.[7] and the detailed data are shown in Supplementary Table S1. Reproduced with permission from John Wiley and Sons. **(c)** The fabrication process of nanocomposite and EA clutch. Al, aluminum; BOPP, biaxially oriented polypropylene; BST, (Ba, Sr) TiO_3; BTO, $BaTiO_3$; DMF, *N,N*-dimethylformamide; EA, electrostatic adhesion; E_{bd}, breakdown field or breakdown strength; Kapton, PI film produced by DuPont; Luxprint, nanocomposite containing BTO particles produced by DuPont; Mylar, polyethylene terephthalate film produced by DuPont; PI, polyimide; PTO, $PbTiO_3$; PVDF, poly(vinylidene fluoride); PZT, $PbZrTiO_3$; STO, $SrTiO_3$; P(VDF-TrFE-CTFE), poly(vinylidene fluoride–trifluoroethylene–chlorotrifluoroethylene); 0.5/1/1.5/2 wt%, composite with 0.5/1/1.5/2 wt% $Ti_3C_2T_x$; ε_r, real part of permittivity or dielectric constant.

dimensional conductive material $Ti_3C_2T_x$ is one kind of exciting nanomaterial created by Naguib *et al.* with atomic-scale thickness and a high aspect ratio.[16] By the hydrofluoric acid (HF) etching method, $Ti_3C_2T_x$ nanosheet is exfoliated and delaminated from its precursor Ti_3AlC_2.

The large flakes up to 4.5 μm, and high conductivity ' $\sim$5500 S/m of $Ti_3C_2T_x$ resulted in a superhigh relative dielectric constant up to 100,000 of $Ti_3C_2T_x$–polymer nanocomposite.[17] The Maxwell–Wagner–Sillars effect in the multicomponent systems causes charge accumulation on the interfaces of polymer matrix and conductive filler, which has been proved to contribute largely to the giant dielectric permittivity.[18]

Fabrication process of dielectrical film and EA clutch

For terpolymer film, P(VDF-TrFE-CTFE) powder (Piezotech S.A., France) and *N,N*-dimethylformamide (DMF) were mixed in a ratio of 14 g:100 mL and dissolved.[7] For the nanocomposite, the fabrication (Fig. 1c) consists of three basic processes: mixing, coating, and curing. The $Ti_3C_2T_x$ was dispersed in DMF in advance to form a 3 mg/mL solution (Beike 2D materials Co., Ltd., China). In the mixing process, P(VDF-TrFE-CTFE) powder was added to $Ti_3C_2T_x$–DMF colloid and dissolved gradually. After ultrasonic treatment for 2 h with an ice bath, the $Ti_3C_2T_x$ nanosheets were dispersed in polymer solution.

Then, the $Ti_3C_2T_x$–polymer solution was coated on the aluminum (Al) side of the aluminized BOPP substrate (70 nm Al layer with 25 μm BOPP layer) to form a 40 μm wet composite layer. The film was compliant due to its super thin thickness. The Al layer was connected to the positive terminal of the power supply in the application.

During the heating process (100°C, 1 h), solvent DMF's evaporation made the film shrink in horizontal and thickness directions. Since the volume of solvent in each sample was same, a constant thickness (17 μm) could always be obtained by the stable scraping technology. The film was curling due to the strain during the material shrinkage. The uneven plane was likely to result in an air gap, greatly weaken the EA force,[19] and aggravate electrical breakdown.[20] PI tape with 45 μm thickness was attached to the BOPP layer to ensure the flatness of the dielectric layer and the tensile resistance of the positive electrode of the clutch. The negative electrode was processed similarly, with Al as the conductive layer and BOPP and PI as substrates (Fig. 1c).

All the experiments involving subjects in this article were approved by the Southern University of Science and Technology, Human Participants Ethics Committee (20210090), and consent was obtained from all participants.

Results and Discussion

Dielectric properties

Temperature scan broadband dielectric spectroscopy (Agilent LCR meter 4980A) was carried out to analyze the dielectric properties of P(VDF-TrFE-CTFE) and composite films. As shown in Figure 2a and b, the real part of permittivity of P(VDF-TrFE-CTFE) increases from 43.38 to 144.38 by 3-fold when the insulator is heated from 30°C to 100°C, along with the rising of the imaginary part from 5.68 to 355.85 by 63-fold. These upturns of ε_r' and ε_r'' at a high temperature can be attributed to the gradually larger movement of the polymer chains as the temperature rises[21] and the migration of impurity ions, which are inherited from the suspension terpolymerization.[22]

These increasing tendencies occur in the composite mixed with $Ti_3C_2T_x$ even more evidently. A higher weight ratio of $Ti_3C_2T_x$ results in a higher dielectric constant (Fig. 2a). The composite with 2 wt% $Ti_3C_2T_x$ reaches a 46.49-fold higher dielectric constant at 100°C (2349.14) than that at 30°C (50.53), which is much more significant than the dielectric constant increase of P(VDF-TrFE-CTFE). Despite the microscopic dipoles distributed on the interfaces between matrix and filler dramatically enhance the dielectric constant,[17] charges at the electrode–dielectric and filler–dielectric interface are activated simultaneously by thermally increasing and injecting into dielectric at high temperature, which consequently causes conduction loss.[23]

Luckily, compared with the real part of the permittivity of composites, the imaginary part increases relatively slowly as the temperature rises (Fig. 2b). Figure 2c illustrates that without $Ti_3C_2T_x$, the loss tangent of the terpolymer rises monotonically from 30°C to 100°C, and the maximum is 2.46 at 100°C. As $Ti_3C_2T_x$ is added in, the maximum loss tangent takes place at a lower temperature, and when the temperature surpasses this value, the loss tangent decreases.

These tendencies are also true for different frequencies (20, 30, 40, 50, and 100 Hz), as shown in Supplementary Figures S1–S3, although the magnitudes are slightly different. When the frequency increases, both the real part and the imaginary part of the permittivity drop since the charge transportation is a time-dependent process. The optimal temperature of the loss tangent reduces when the frequency decreases.

The real part of permittivity increases by 54 times, which might result in a stronger output force according to Equations (3) and (4), as well as decreases the expense or weight of the high voltage generator since very high voltage is no longer needed, although a higher leakage current could also be caused. Moreover, operating at a specific high temperature (e.g., > 70°C), the loss tangent of the clutch with nanocomposite as dielectric layer falls down to a lower value (Fig. 2c).

Force density

The direct current (DC) breakdown strength and capacitance–voltage (C-V) curve of the samples were measured using a modified Sawyer–Tower circuit with artificial intelligence control (Polyk Technologies) and Trek Model 20/20C ± 20 kV high voltage amplifier system. The temperature was controlled utilizing an oil bath heating device equipped with a thermal couple. For each kind of film under each temperature, five samples were evaluated (Supplementary Table S2) and the maximum was used for the following analysis. For P(VDF-TrFE-CTFE), the maximum breakdown field declines consistently as the temperature rises from 30°C to 100°C (Fig. 2d).

That is because the interaction of electrical, thermal, and mechanical factors at high temperatures decreases the energy barrier and causes the polymer to easily break down.[24] After adding $Ti_3C_2T_x$, the breakdown field falls more slowly as temperature rises. That is probably because the $Ti_3C_2T_x$ nanosheets near the surface of composite are oxidized to TiO_2, which generates a higher charge trap density and prevents charge transportation in films by trapping charges injected from electrodes.[25] The different weight ratios of $Ti_3C_2T_x$ result in a little discrepancy in the breakdown field,

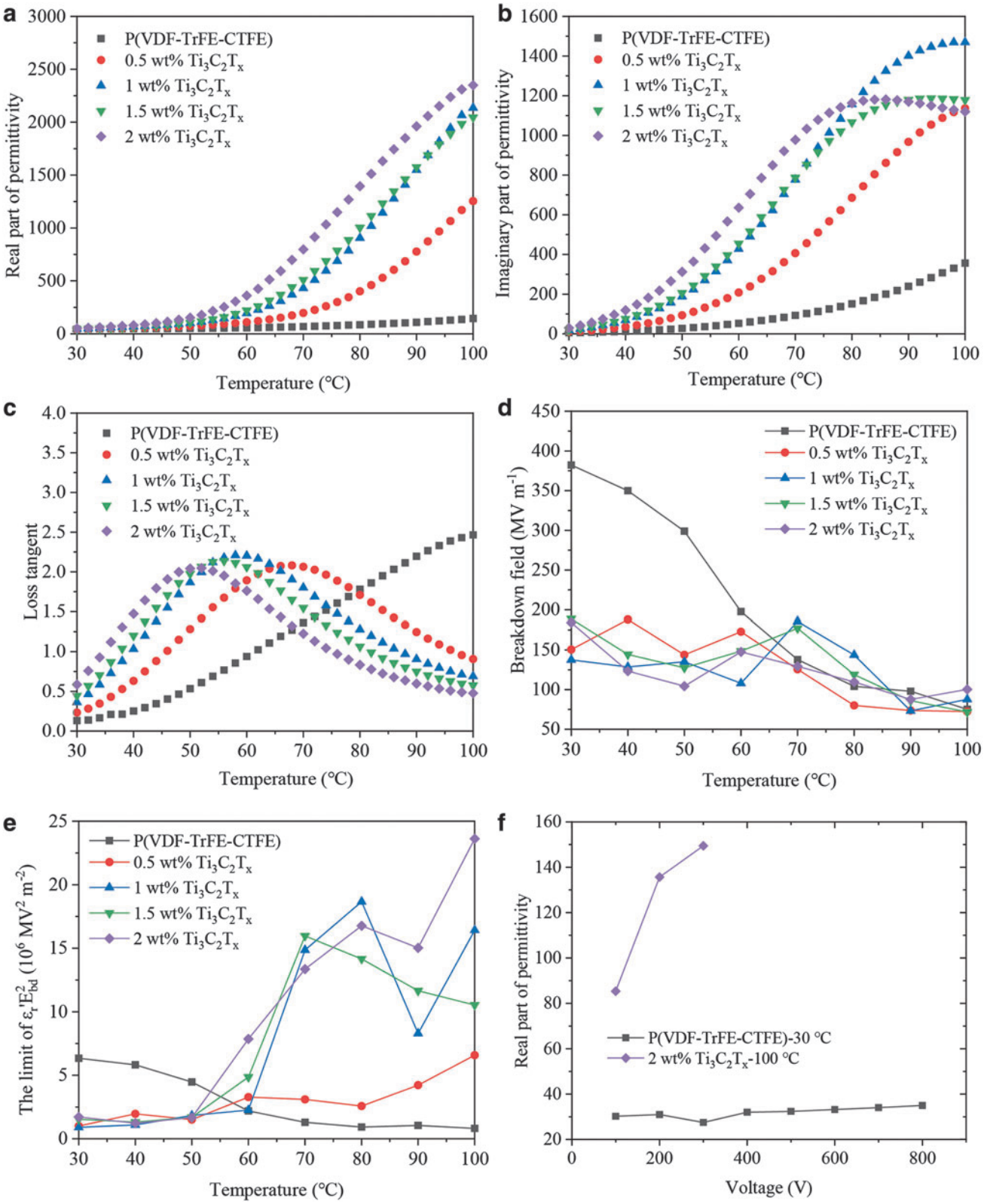

FIG. 2. Dielectric properties of terpolymer and nanocomposite. **(a)** The real part of permittivity, **(b)** the imaginary part of permittivity, and **(c)** the loss tangent at 20 Hz, 0.5 V bias. **(d)** Breakdown field. **(e)** Limit of $\varepsilon_r E_{bd}^2$. **(f)** The real part of permittivity at 10 Hz, 100–800 V bias.

and finally, the composites possess a comparable breakdown electrical field with P(VDF-TrFE-CTFE) at 70–100°C.

Based on the experimental data already mentioned, we calculate $\varepsilon_r' E_{bd}^2$ of each material, and the results are shown in Figure 2e. Despite that ε_r' could be influenced by field strength, it is a common method to compare the value at the same low voltage to facilitate the comparison between different materials.[4,7,8] For P(VDF-TrFE-CTFE), the value of $\varepsilon_r' E_{bd}^2$ declines monotonically as the temperature increases, whereas for composites, it generally increases.

For example, in the composite with 0.5 wt% $Ti_3C_2T_x$, $\varepsilon_r' E_{bd}^2$ increases by 6.57-fold from 30°C to 100°C. With more $Ti_3C_2T_x$ (1–2 wt%), it increases more drastically, particularly in the range of 50°C to 70°C. The maximum $\varepsilon_r' E_{bd}^2$ finally reaches 23.63×10^6 MV^2/m^2 at 100°C. Compared with P(VDF-TrFE-CTFE), composite possesses a considerably higher $\varepsilon_r' E_{bd}^2$, and thus we can generate a stronger EA force by increasing the temperature.

In many other literature regarding polymer-based conductive sheet-filled composite, despite authors declaring that their samples, such as V_2C/ZnS/P(VDF-TrFE)[26] and $Ti_3C_2T_x$/PVDF[27] exhibit balanced dielectric constant and breakdown field, the values of $\varepsilon_r' E_{bd}^2$ are only 2.12×10^6 and 3.30×10^6 MV^2/m^2, which are quite lower than 23.63×10^6 MV^2/m^2. Considering most of the electroadhesive devices are made of polymers and polymer composites, our result will certainly motivate the development of higher performance composite. It is worth mentioning that by improving the interfacial polarization[28] and fabricating better dispersed nanomaterial with fewer defects,[29,30] the dielectric constant and breakdown field can be improved, respectively, and thus increases $\varepsilon_r' E_{bd}^2$ furthermore.

We measured the EA shear stress by the setup shown in Figure 3a. The positive electrode with a dielectric layer was attached to one side of an Al board anchored to the ground. On the other side of the Al board, a heat plate made of PI basement and copper wires was bonded. A temperature control box (Mijiang Technology WK7016C1, China) tuned the temperature to the target with the feedback from a temperature sensor.

The negative electrode was connected to the moving stage of a tensile tester (ZHIQU-990B, China) through a 50 N load cell (Zwjnsensor JLBS-M2, China). During the test, the moving stage pulled the negative electrode up at a constant speed of 10 mm/min, after voltage (Trek Model 615-3 DC/AC generator) was provided to the EA clutch. To eliminate the accumulation of surface charges, we applied a bipolar rectangular AC voltage signal (10 Hz).[7]

According to the results shown in Figure 2e, we take several special conditions (terpolymer at 30°C, the composite with 0.5 wt% $Ti_3C_2T_x$ at 100°C, the composite with 1 wt% $Ti_3C_2T_x$ at 80°C, the composite with 1.5 wt% $Ti_3C_2T_x$ at 70°C, and the composite with 2 wt% $Ti_3C_2T_x$ at 100°C) for further comparison of EA force density, and the thickness of all samples is 17 μm. As shown in Figure 3b, the composite obtained the largest stress (85.61 N/cm^2) with 1.5 wt% $Ti_3C_2T_x$ at 500 V and 70°C, ~4 times higher than the maximum value (21 N/cm^2, obtained at 12.5 μm thickness) achieved in the past (Supplementary Fig. S4).[7,8,10,31–34]

Derived from the C–V curve, the relative dielectric constant could be affected by voltage (Fig. 2f). Compared with the terpolymer, the composite (2 wt% $Ti_3C_2T_x$) has a much apparent increasing trend. The dielectric constant of composite finally reaches 149.47 at 300 V (10 Hz) and 100°C, 5.44-fold higher than the terpolymer (27.47) at the same voltage and 30°C. This result is roughly coincident with the result of EA shear stress shown in Figure 3b, in which these two samples exist a 3.10× relationship, 71.87 N/cm^2 for composite at 300 V and 100°C, and 23.22 N/cm^2 for terpolymer at 300 V and 30°C.

Note that in Figure 3b, the slope of most curves declines once the breakdown voltage approaches. That is perhaps because tiny discharge occurs before the breakdown voltage, and the clutch pair can still adsorb together. Moreover, for unfilled terpolymer, high temperature worsens the EA shear stress (Fig. 3c). It suggests that our composites are effective to elevate the EA shear stress. The average off-state friction of the composite clutch at 70°C (Fig. 3d) is only 0.0039 N/cm^2, indicating the viscous force between the clutch pair can be neglected. The engage and release times of the composite clutch at 200 V AC and 70°C (Fig. 3e, f) were also measured. The clutch takes <50 ms to engage and ~37 ms to release, which is comparable with the previous literature.[10]

Electrical properties

As already mentioned, the composite can strengthen the EA force density but might sacrifice the electrical properties, for example, the leakage current and power consumption, simply because some of the interfaces of $Ti_3C_2T_x$ inevitably overlap with each other and form conductive paths.[35] Here we evaluate the leakage current and resistivity of film materials using a Keysight megger (B2985A) with a PolyK high-voltage testing system (PK-SPIV17T-158A). As shown in Figure 4a, the leakage current of the composite keeps stably at <0.1 μA for different electrical fields, which is still acceptable.

This magnitude is close to the leakage current of P(VDF-TrFE-CTFE) and poly(vinylidene fluoride–trifluoroethylene–chlorofluoroethylene) [P(VDF-TrFE-CFE)], although it is approximately three orders higher than that of PI, which is extensively employed as the dielectric layer in EA.[8,36] The corresponding volume resistivity is calculated from the leakage current by Ohm's law, and the results are shown in Figure 4b. The volume resistivity of the composite surpasses 2GΩ, only three orders lower than that of PI.

The sheet resistivity of six kinds of materials, including conductors and insulators, is also studied (Fig. 4c). For insulators, a Keysight megger with a probe station (Cindbest CS-4, China) was employed, whereas for conductors, a probe table surface resistance tester (four probes) (Model 280SI, Canada) was used. The sheet resistivity of frequently used dielectric materials such as PI, Luxprint (DuPont), and P(VDF-TrFE-CTFE) is $\sim 10^{14}$ Ω/sq^{-1}. The sheet resistivity of the composite with 2 wt% $Ti_3C_2T_x$ is a little bit lower ($\sim 10^{13}$ Ω/sq^{-1}), but still >12 orders higher than the conductors such as Al and steel.

We also evaluated the average power of EA clutches made of P(VDF-TrFE-CTFE) and composite (1.5 wt% $Ti_3C_2T_x$) (1.5 cm^2) by an electrometer (Keithley 6514). We first measured the voltage and the current. As shown in Figure 4d, the instantaneous current peaks (maximum current) right after the voltage changes sharply, and then it drops to a considerably lower value (leakage current). The average power is calculated according to

$$P = \frac{1}{T}\int_0^T uidt, \tag{5}$$

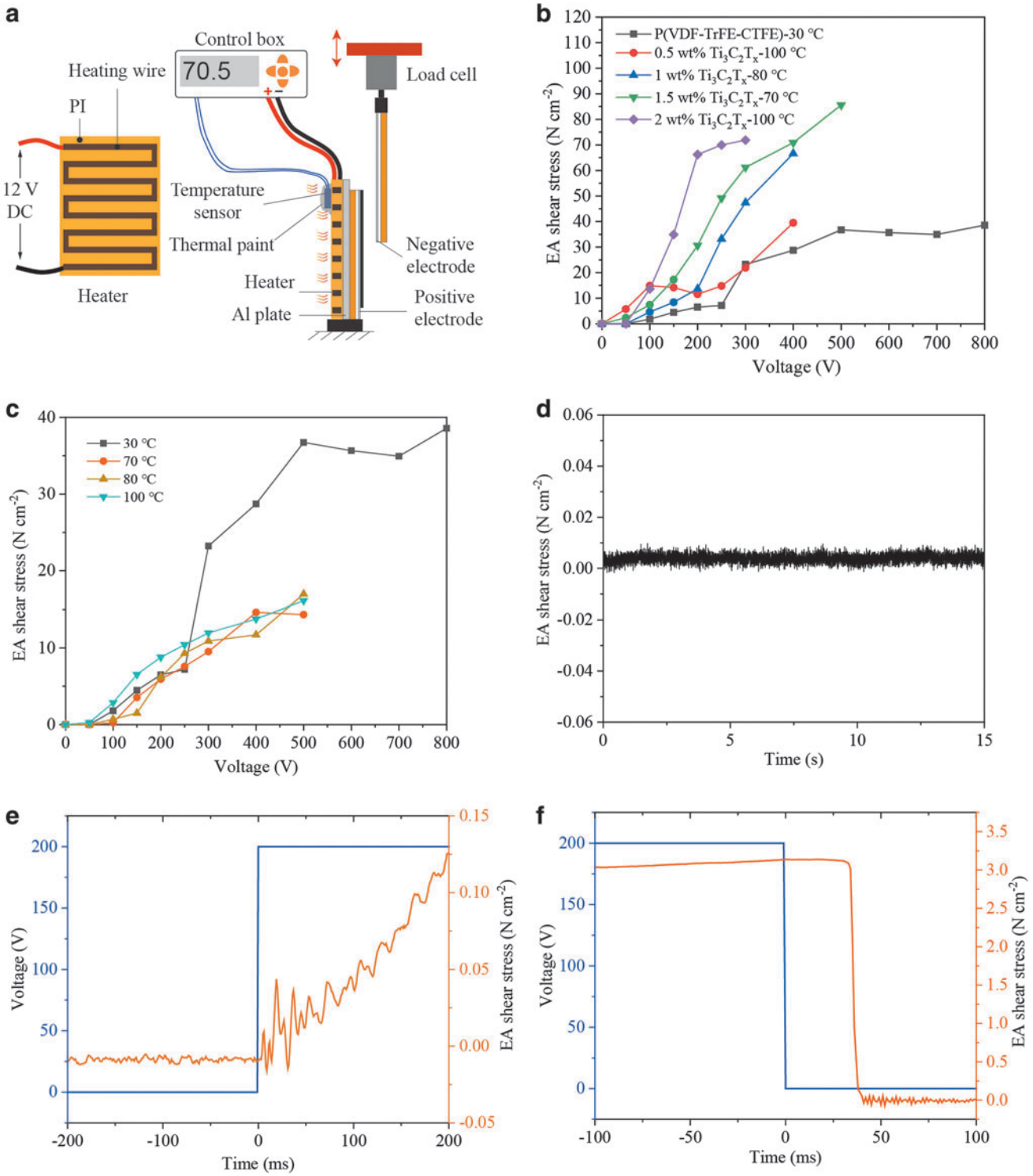

FIG. 3. Force density and response time measurement. **(a)** The device for EA shear stress testing. **(b)** The EA shear stress of P(VDF-TrFE-CTFE) and composites. **(c)** The EA shear stress of P(VDF-TrFE-CTFE) at 30°C and high temperatures. **(d)** The off-state EA shear stress of the composite (1.5 wt% $Ti_3C_2T_x$) clutch at 70°C. **(e)** The engage time and **(f)** the release time of the composite (1.5 wt% $Ti_3C_2T_x$) clutch at 70°C and 200 V AC. AC, alternating current; DC, direct current.

where u and i are the instantaneous voltage and current of the EA clutch, respectively. T is the total time. As shown in Figure 4e, the average power consumption per square centimeter of the clutch increases exponentially along with the applied voltage for both P(VDF-TrFE-CTFE) and the composite, but at the same voltage, the value of P(VDF-TrFE-CTFE) is about a quarter of the counterpart of composite. On 500 V AC voltage, the clutch made from the composite consumes 45.15 mW/cm^2 power, which is still acceptably low for most robotics applications.

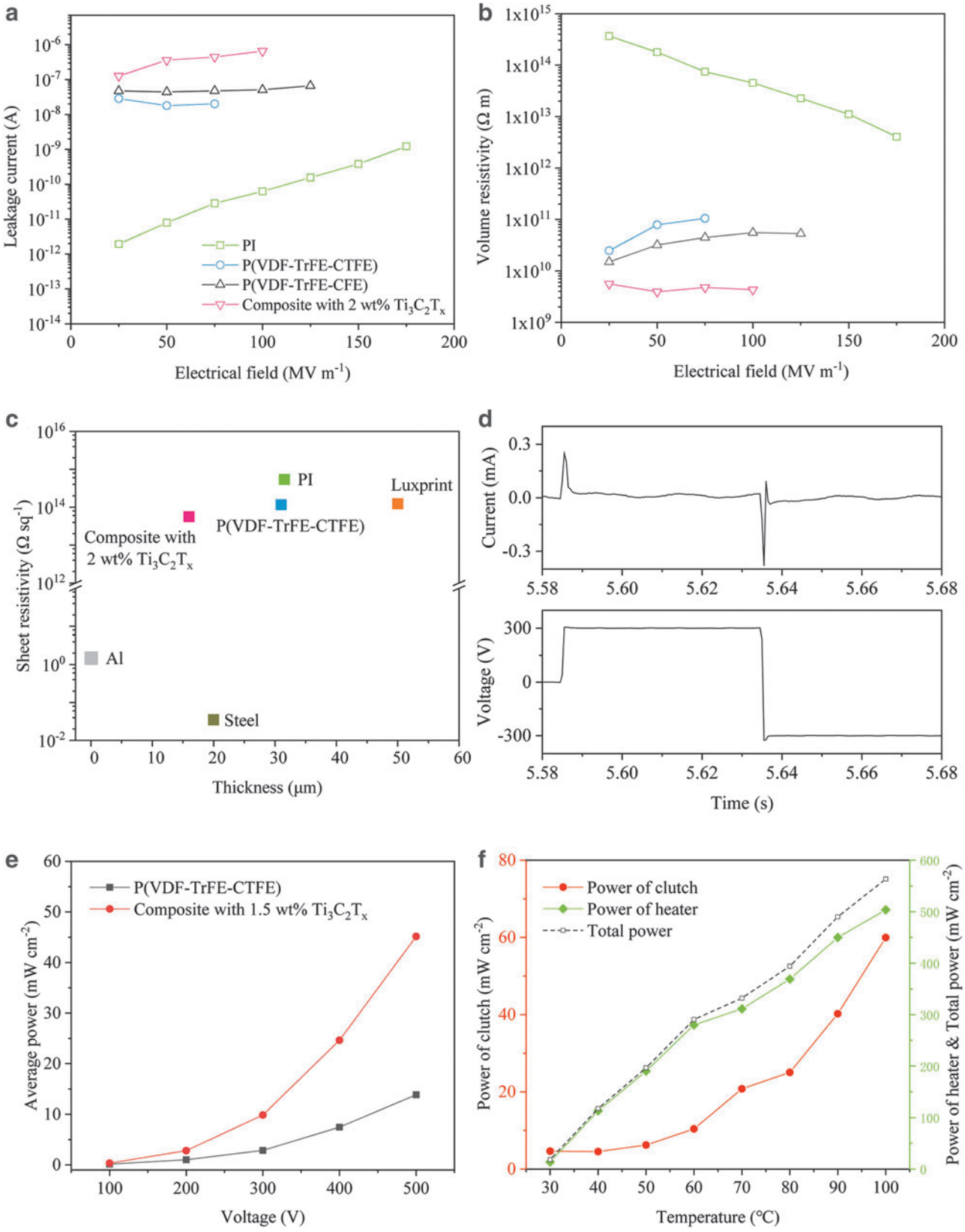

FIG. 4. Electrical properties. **(a)** The leakage current, **(b)** the volume resistivity, and **(c)** the sheet resistivity at room temperature. **(d)** Instantaneous voltage and current of EA clutch at room temperature. **(e)** The average power of EA clutch with P(VDF-TrFE-CTFE) and composite at different voltage and room temperature. **(f)** The power consumption of the EA clutch with composite (1.5 wt% $Ti_3C_2T_x$) and heater at different temperatures as well as the total power. P(VDF-TrFE-CFE), poly (vinylidene fluoride–trifluoroethylene–chlorofluoroethylene).

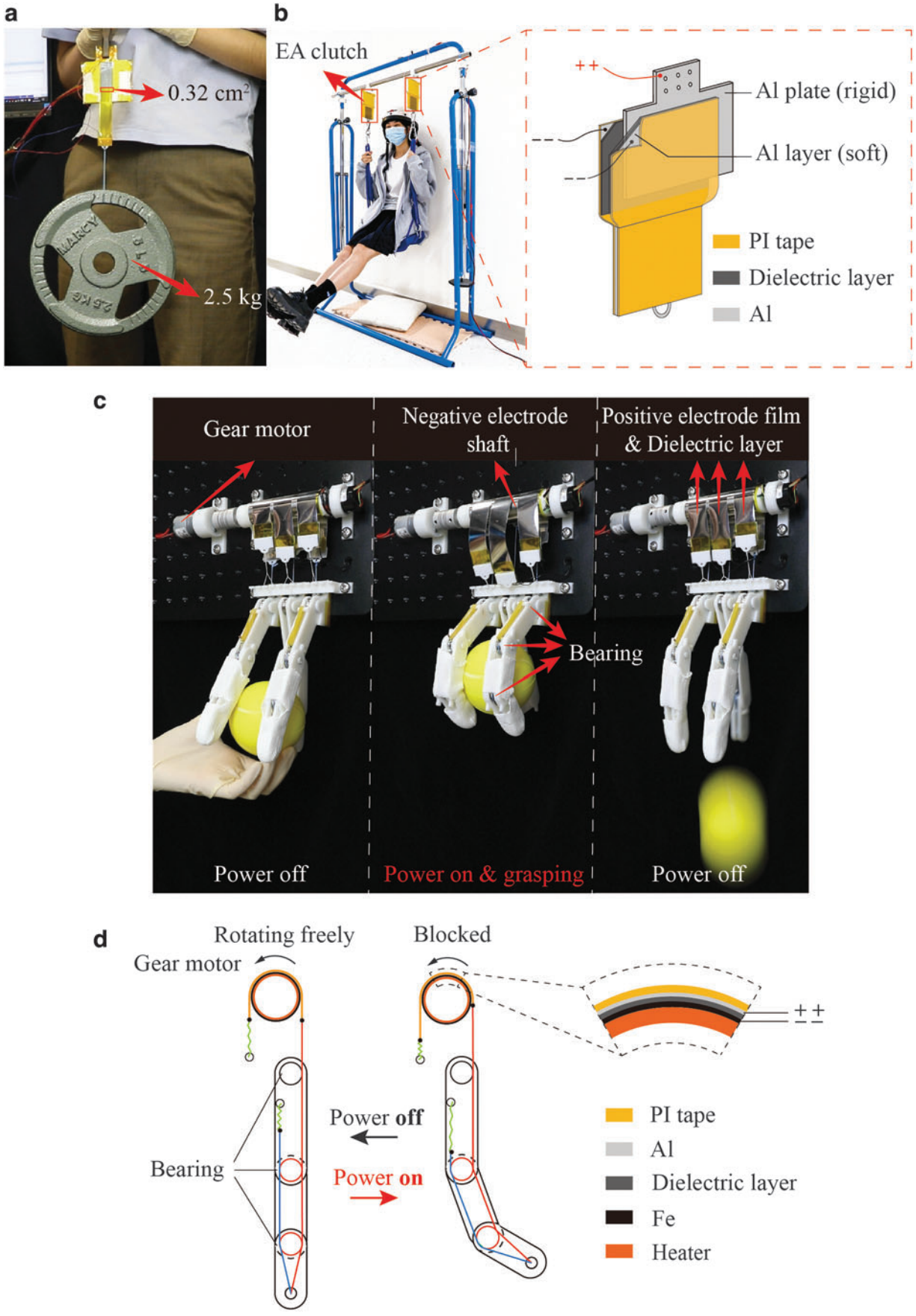

FIG. 5. Demonstrations. **(a)** EA clutch of 0.32 cm^2 overlapping area holds 2.5 kg weight. **(b)** EA clutch holds an adult female (45 kg) and the diagram of the EA clutch. **(c)** A robotic hand actuated by the EA clutch grasps a ball and releases it. **(d)** Structural diagram of the robotic hand. Fe, iron.

While the temperature rises, the average power increases by >10 times (from 4.63 mW/cm^2 at 30°C to 59.97 mW/cm^2 at 100°C) under 300 V (Fig. 4f). To create a fair comparison to alternative device solutions, the per area power consumption of heater is also considered and the total power at 100°C is 565.55 mW/cm^2 (Fig. 4f).

Demonstrations

With superhigh force density, the material proposed here for electrostatic device is applicable in more extensive application fields. For example, our clutch can hold a 2.5 kg disk by an overlapping area of only 0.32 cm^2 (1.6×0.2 cm^2, 500 V, 70°C) (Fig. 5a and Supplementary Video S1). With more area, for example, 380 cm^2, the electrostatic clutch stably hangs up an adult lady (45 kg) on a swing (Fig. 5b left and Supplementary Video S2). To prevent stretching failure, we utilize a smooth Al plate as the positive electrode and a dielectric layer with a thicker substrate as the negative electrode (Fig. 5b right).

Considering the safety in application, the BOPP and PI substrates can also prevent haptic device users from shock, since they isolate the skin from the electrodes. Furthermore, high-voltage devices were already used in haptics devices and in some medical devices, which require high safety.[8,37] In the future, we will limit the maximum current to <1 mA, which is a safe threshold for humans.[38]

The electrostatic clutch can also be applied to robotics. In this study, we design a robotic hand of three fingers integrating electrostatic clutches, as shown in Figure 5c, d and Supplementary Video S3. In this device, a grounding rotation shaft (iron) driven by a gear motor was connected as the negative electrode. Three pieces of electrode films (electrodes covered by nanocomposite) were connected to three fingers by string, respectively. The electrode films were placed on the curvature of the shaft, and their electrodes were connected to positive voltage. To avoid the tangling, a conductive slip ring (MSC-22-0605A, MSLIPRING) was used to connect the rotating wires (for ground and heater) and fix wires.

The conductive slip ring consisted of a stator that was fixed and mounted on the base, and a rotor that could rotate with the rotating shaft. The stator was connected to the rotor. Without electrical power, electrode films slipped on the rotating shafts since there was no attraction between them. Only the electrical motor and the shaft rotated, but the fingers kept free. After an AC voltage was applied to the electrodes, the electrode films adhered to the rotating shaft and pulled the fingers to bend, and consequently, the three bending fingers closed the hand and grasped a ball. Once the power on the clutch was cut off, the fingers were released, and the object dropped. This demonstration shows the controllability of the electrostatic clutch and its application in smart mechatronics systems.

Conclusions

In this article, the manufacturing approach related to dielectric nanocomposite with ultrahigh dielectric constant while without deteriorated breakdown strength, followed by the fabrication of soft clutch has been reported. We propose that the whole value of $\varepsilon_r' E_{bd}^2$ takes main responsibility for the upper limitation of electrostatic attraction. By compositing $Ti_3C_2T_x$ with terpolymer P(VDF-TrFE-CTFE), we obtain nanocomposite films with a dielectric constant of >2300 at 100°C.

Typically, the $\varepsilon_r' E_{bd}^2$ value of the composite at 70–100°C is reached to about three times the counterpart of P(VDF-TrFE-CTFE) at 30°C. The clutch using this nanocomposite as a dielectric layer has EA shear stress of 85.61 N/cm^2 at 500 V and 70°C, despite there being increase in power consumption.

We believe that by deploying a temperature control system to keep the temperature for the maximum dielectric constant of the dielectric layer, the clutch could be operated in harsh environments such as spaces with ultrahigh or low temperatures and polar regions including Arctic, Antarctic, snow mountain, and ice field. EA is an interdisciplinary field with vast potential to investigate. With physics, chemistry, material, mechanics, and electricity integrated into this research, its future application scenarios should include but not be limited to grippers, climbing robotics, and haptic device.

Author Disclosure Statement

No competing financial interests exist.

Funding Information

This study is supported by the National Natural Science Foundation for Young Scientists of China (51905256), the Natural Science Foundation of Guangdong Province of China (2020A1515010955), the Natural Science Foundation of Liaoning Province of China (State Key Laboratory of Robotics joint funding, 2021-KF-22-11), the Science, Technology and Innovation Commission of Shenzhen Municipality (ZDSYS20200811143601004), and the Southern Marine Science and Engineering Guangdong Laboratory (Guangzhou) (K19313901).

Supplementary Material

Supplementary Table S1
Supplementary Table S2
Supplementary Figure S1
Supplementary Figure S2
Supplementary Figure S3
Supplementary Figure S4
Supplementary Video S1
Supplementary Video S2
Supplementary Video S3

References

1. Johnsen A, Rahbek K. A physical phenomenon and its applications to telegraphy, telephony, etc. J Inst Electr Eng 1923;61:713–725.
2. Shintake J, Rosset S, Schubert B, *et al.* Versatile soft grippers with intrinsic electroadhesion based on multifunctional polymer actuators. Adv Mater 2016;28:231–238.
3. Boutilier MSH, Cao C, Nayakanti N, *et al.* Limiting mechanisms and scaling of electrostatically controlled adhesion of soft nanocomposite surfaces for robotic gripping. ACS Appl Mater Interfaces 2021;13:1192–1203.
4. Wang H, Yamamoto A, Higuchi T. A crawler climbing robot integrating electroadhesion and electrostatic actuation. Int J Adv Robot Syst 2014;11:1–11.
5. Wang H, Yamamoto A. Analyses and solutions for the buckling of thin and flexible electrostatic inchworm climbing robots. IEEE Trans Robot 2017;33:889–900.
6. Sirbu ID, Moretti G, Bortolotti G, *et al.* Electrostatic bellow muscle actuators and energy harvesters that stack up. Sci Robot 2021;6:eaaz5796.

7. Hinchet R, Shea H. High force density textile electrostatic clutch. Adv Mater Technol 2020;5:1–7.
8. Hinchet R, Vechev V, Shea H, *et al.* Dextres: Wearable haptic feedback for grasping in VR via a thin form-factor electrostatic brake. In: UIST 2018-Proceedings of the 31st Annual ACM Symposium on User Interface Software Technology. New York, NY, United States: Association for Computing Machinery, 2018;901–912.
9. Gupta U, Qin L, Wang Y, *et al.* Soft robots based on dielectric elastomer actuators: A review. Smart Mater Struct 2019;28:103002.
10. Diller S, Majidi C, Collins SH. A lightweight, low-power electroadhesive clutch and spring for exoskeleton actuation. In: IEEE International Conference on Robotics and Automation. Stockholm, Sweden: IEEE, 2016.
11. McPherson J, Kim JY, Shanware A, *et al.* Thermochemical description of dielectric breakdown in high dielectric constant materials. Appl Phys Lett 2003;82:2121–2123.
12. Jain P, Rymaszewski EJ. Embedded thin film capacitors—Theoretical limits. IEEE Trans Adv Packag 2002;25:454–458.
13. Guo M, Jiang J, Shen Z, *et al.* High-energy-density ferroelectric polymer nanocomposites for capacitive energy storage: Enhanced breakdown strength and improved discharge efficiency. Mater Today 2019;29:49–67.
14. Zhai Y, Zhang Y, Ren W. Electromagnetic characteristic and microwave absorbing performance of different carbon-based hydrogenated acrylonitrile-butadiene rubber composites. Mater Chem Phys 2012;133:176–181.
15. Wei J, Zhu L. Intrinsic polymer dielectrics for high energy density and low loss electric energy storage. Prog Polym Sci 2020;106:101254.
16. Naguib M, Kurtoglu M, Presser V, *et al.* Two-dimensional nanocrystals produced by exfoliation of Ti3AlC2. Adv Mater 2011;23:4248–4253.
17. Tu S, Jiang Q, Zhang X, *et al.* Large dielectric constant enhancement in MXene percolative polymer composites. ACS Nano 2018;12:3369–3377.
18. Yuan JK, Yao SH, Dang ZM, *et al.* Giant dielectric permittivity nanocomposites: Realizing true potential of pristine carbon nanotubes in polyvinylidene fluoride matrix through an enhanced interfacial interaction. J Phys Chem C 2011;115:5515–5521.
19. Xie G, Wang W, Zhao X, *et al.* Low-voltage electroadhesive pad with thin insulation layer fabricated by parylene deposition. In 2019 IEEE 9th Annual International Conference on CYBER Technology in Automation, Control, and Intelligent Systems. Suzhou, China: IEEE, 2019.
20. Mardikyan K. Breakdown strength of air, SF6 and a mixture of air plus SF6 containing a small amount of SF6. Eur Trans Electr Power 1999;9:1–4.
21. Haq YU, Murtaza I, Mazhar S, *et al.* Investigation of improved dielectric and thermal properties of ternary nanocomposite PMMA/MXene/ZnO fabricated by in-situ bulk polymerization. J Appl Polym Sci 2020;137:49197.
22. Yang L, Tyburski BA, Dos Santos FD, *et al.* Relaxor ferroelectric behavior from strong physical pinning in a poly(vinylidene fluoride-co-trifluoroethylene-co-chlorotrifluoroethylene) random terpolymer. Macromolecules 2014;47:8119–8125.
23. Dong J, Hu R, Xu X, *et al.* A facile in situ surface-functionalization approach to scalable laminated high-temperature polymer dielectrics with ultrahigh capacitive performance. Adv Funct Mater 2021;31:1–9.
24. Shen ZH, Wang JJ, Jiang JY, *et al.* Phase-field modeling and machine learning of electric-thermal-mechanical breakdown of polymer-based dielectrics. Nat Commun 2019;10:1–10.
25. Dall'Agnese C, Dall'Agnese Y, Anasori B, *et al.* Oxidized Ti3C2 MXene nanosheets for dye-sensitized solar cells. New J Chem 2018;42:16446–16450.
26. Deng Q, Xiong W, Mao B, *et al.* Enhanced dielectric response of ternary polymeric composite films via interfacial bonding between V2C MXene and wide-bandgap ZnS. Ceram Int 2021;47:32938–32946.
27. Li W, Song Z, Zhong J, *et al.* Multilayer-structured transparent MXene/PVDF film with excellent dielectric and energy storage performance. J Mater Chem C 2019;7:10371–10378.
28. Samet M, Kallel A, Serghei A. Polymer bilayers with enhanced dielectric permittivity and low dielectric losses by Maxwell–Wagner–Sillars interfacial polarization: Characteristic frequencies and scaling laws. J Appl Polym Sci 2019;136:38–40.
29. Jahoda E, Kudelcik J, Hornak J, *et al.* The influence of nanoparticles in the epoxy resin on dielectric parameters and partial discharges. In 2018 ELEKTRO. Mikulov, Czech Republic: IEEE, 2018;1–5.
30. Calebrese C, Hui L, Schadler LS, *et al.* A review on the importance of nanocomposite processing to enhance electrical insulation. IEEE Trans Dielectr Electr Insul 2011;18:938–945.
31. Ramachandran V, Shintake J, Floreano D. All-fabric wearable electroadhesive clutch. Adv Mater Technol 2019;4:1–7.
32. Chen AS, Bergbreiter S. A comparison of critical shear force in low-voltage, all-polymer electroadhesives to a basic friction model. Smart Mater Struct 2017;26:25028.
33. Diller SB, Collins SH, Majidi C. The effects of electroadhesive clutch design parameters on performance characteristics. J Intell Mater Syst Struct 2018;29:3804–3828.
34. Karagozler ME, Campbell J, Fedder GK, *et al.* Electrostatic latching for inter-module adhesion, power transfer, and communication in modular robots. In: IEEE/RSJ International Conference on Intelligent Robots and Systems. San Diego, CA, USA: IEEE, 2007.
35. Wang Y, Li Y, Wang L, *et al.* Gradient-layered polymer nanocomposites with significantly improved insulation performance for dielectric energy storage. Energy Storage Mater 2020;24:626–634.
36. Gu G, Zou J, Zhao R, *et al.* Soft wall-climbing robots. Sci Robot 2018;3:eaat2874.
37. Palanker D, Vankov A, Jayaraman P. On mechanisms of interaction in electrosurgery. New J Phys 2008;10:123022.
38. Fish RM, Geddes LA. Conduction of electrical current to and through the human body: A review. Eplasty 2009;9:e44.

Address correspondence to:
Hongqiang Wang
Department of Mechanical and Energy Engineering
Southern University of Science and Technology
Shenzhen 518055
China

E-mail: wanghq6@sustech.edu.cn

Hong Wang
Department of Materials Science and Engineering
Southern University of Science and Technology
Shenzhen 518055
China

E-mail: wangh6@sustech.edu.cn